

Dynamic foot morphology explained through 4D scanning and shape modeling

Abhishektha Boppana^{a,*}, Allison P. Anderson^a

^a*Ann and H.J. Smead Department of Aerospace Engineering Sciences, University of Colorado Boulder, USA*

5

Abstract

Having a proper understanding of foot morphology can help design more comfortable and better fitting footwear. However, foot morphology is highly variable within the population, and can vary when the foot is loaded during stance phase. This study aims to develop a parametric statistical shape model from 4D foot scans to capture both the inter- and intra-individual variability in foot morphology. Thirty subjects walked on a treadmill while 4D scans of their right foot were taken at 90 frames-per-second during stance phase. Each subject's height, weight, foot length, foot width, arch length, and sex were also recorded. The 4D scans were all registered to a common high-quality foot scan, and a principal component analysis was done on all processed 4D scans. Elastic-net linear regression models were built to predict the principal component scores, which were then inverse transformed into 4D scans. The best performing model was selected with leave-one-out cross-validation. The chosen model was able to predict foot morphology across stance phase with a root-mean squared error of 5.74 ± 2.30 mm. This study shows that statistical shape modeling can be used to predict dynamic changes in foot morphology across the population. The model can be used to investigate and improve foot-footwear interaction, allowing for better fitting and more comfortable footwear.

Keywords: foot morphology, dynamic scanning, gait biomechanics, shape modeling

10

1. Introduction

Foot shape is known to be highly variable throughout the population, including by sex (Wunderlich and Cavanagh 2001; Krauss et al. 2008, 2010), age (Tomassoni, Traini, and Amenta 2014), and weight (Price and Nester 2016).
15 This variability is often not captured in footwear sizing, as current footwear fitting standards only use foot length, foot width, and arch length to fit to standardized shoe sizes (“Standard Practice for Fitting Athletic Footwear” 2017).

*Corresponding Author
Preprint submitted to Journal of Biomechanics
Email addresses: abhishektha@colorado.edu (Abhishektha Boppana), July 13, 2020
apanders@colorado.edu (Allison P. Anderson)

Furthermore, footwear is commonly designed around lasts, shoe molds that are sized and shaped by each manufacturer with no common standard, leading to variability in footwear shapes and sizes (Jurca and Dzeroski 2013; Wannop et al. 2019). Such variability can make it hard for consumers to find a proper fit, resulting in users having to wear ill-fitting footwear with suboptimal comfort (Dobson et al. 2018). Footwear comfort has shown benefits in increasing running performance (Luo et al. 2009) and reducing the risk of movement-related injury (Mündermann, Stefanyszyn, and Nigg 2001), and is often the number one (Martínez-Martínez et al. 2017) factor for consumers to select footwear. Footwear should therefore be properly fit to a wide population range in order to be successful.

However, because the current methodology of designing footwear relies on using static lasts, this assumes that the foot consists of rigid segments. This fails to account for dynamic changes in foot morphology, especially when the foot is being loaded during gait. Assumptions of rigid foot segments during foot loading have shown inaccuracies in estimation of ankle joint mechanics (Zelik and Honert 2018; Kessler et al. 2020), suggesting intra-foot motion as the foot is loaded (Lundgren et al. 2008; Wolf et al. 2008). Evidence suggests that foot loading affects linear foot measurements, such as when transitioning from sitting to standing (Xiong et al. 2009; Oladipo, Bob-Manuel, and Ezenatein 2008) or during the stance phase of gait (Kouchi, Kimura, and Mochimaru 2009; Barisch-Fritz et al. 2014a; Grau and Barisch-Fritz 2018). The dynamically changing measurements suggest morphological changes occurring, all of which may not be captured in static linear and circumferential measurements. Thus, it becomes difficult to characterize the wide variety of foot shapes across not only a large population, but within individuals as their foot goes through loading scenarios such as gait.

Statistical shape models (SSMs) can explain morphological differences across populations by identifying shape modes which account for variance from the mean foot,. These have been developed for whole-body digital human modeling applications to study population and individual variance in body shape (Allen, Curless, and Popović 2003; Anguelov et al. 2005; Reed et al. 2014; Park and Reed 2015; Park, Ebert, and Reed 2017). Parametric SSMs are extensions which use correlations between subject anthropometric data and SSM deformations to help predict body shape for new individuals in the population (Park and Reed 2015; Park, Ebert, and Reed 2017).

SSMs have recently been applied to characterize static foot shape across a population (Conrad et al. 2019) and recognize foot-shape deviations (Stanković et al. 2020). The aforementioned efforts to capture foot measurement changes over the gait cycle did capture 4D foot images (Barisch-Fritz et al. 2014a; Grau and Barisch-Fritz 2018), but these efforts were not translated into a SSM. All the previously developed systems were also based on a catwalk, requiring subjects to correctly hit the scanning area for a successful data capture, which may not be representative of natural cadence.

The development of the DynaMo software (Boppana and Anderson 2019) for the Intel RealSense D415 Depth Cameras (Intel, Santa Clara CA) allowed a

4D scanning system to be set around a treadmill, where subjects can maintain a natural cadence. This system captures the majority of the foot's dorsal surface, but does not allow for the capture of the foot's plantar surface. 4D scans are captured at 90 fps, enabling a detailed evaluation of foot morphology changes during loading and unloading. This study outlines the development of a parametric SSM, derived from scans captured with this system. The parametric SSM can characterize and predict dynamic foot morphology at specific points during stance phase across the subject population. We hypothesize that there will be significant changes in foot morphology across the dorsal surface of the foot throughout the gait cycle. We also hypothesize that these changes will be predictable from the subject demographics of our population.

2. Methods

2.1. Subjects

A total of 30 healthy subjects (15 men and 15 women, ages 23.1 ± 3.7) participated in this study. Subjects were recruited in a stratified sample into one of six groups (5 subjects per group) to maximize variance in population foot length. Height was used as the grouping factor since height is well correlated to foot length (Giles and Vallandigham 1991). The general population may not know offhand their exact foot length, and shoe size varies by manufacturer and does not correspond directly to foot length (Jurca and Dzeroski 2013; Wannop et al. 2019). Groups consisted of 5th-35th, 35th-65th, and 65th-95th height percentiles for each sex. Height percentile values were taken from the ANSUR II survey (Gordon et al. (2014)) and converted to imperial units as it was expected most subjects would report their height in imperial units. Population recruitment groups are summarized in tbl. 1.

Prior to recruitment, subjects completed a prescreening survey to ensure they were adequately healthy by the American College of Sports Medicine guidelines(Riebe et al. 2015), and between the ages of 18-65. Subjects provided their sex and height, and were only enrolled in the study if their population group was not fully enrolled.

Table 1: Enrollment groups based on reported height. 5 subjects were enrolled in each group

Sex	5th-35th percentile Height	35th-65th percentile Height	65th-95th percentile Height
Female	4'11"-5'3"	5'3"-5'5"	5'5"-5'8"
Male	5'4"-5'8"	5'8"-5'11"	5'11"-6'2"

2.2. Experimental Procedures

The experimental protocol was approved by the University of Colorado Institutional Review Board. Procedures were explained to each subject and written consent was obtained prior to participation. Subjects' height and weight were recorded with a tape measure and scale, respectively. Subjects' foot length,

foot width, and arch length were measured with a Brannock device (The Brannock Device Company, Liverpool, NY) (“Standard Practice for Fitting Athletic Footwear” 2017). Both foot length and arch length were measured in centimeters. Foot width was measured as an ordinal size (e.g. A, B, C, D, E), and then converted to a linear measurement in centimeters using the following formula (The Brannock Device Company, Liverpool, NY):

$$w_{cm} = (3 + (w_{offset} * 3/16) + (l * (1/2.54) - 8) * 3/8) * 2.54$$

where w_{cm} is the foot width in centimeters, w_{offset} is the foot width size offset from standard size D, and l is the foot length in centimeters.

Six Intel RealSense D415 Depth Cameras (Intel, Santa Clara, CA) were placed and calibrated around a custom-built level treadmill in the University of Colorado Boulder Locomotion Laboratory, as shown in fig. 1. The DynaMo software package was used to capture depth images of the right foot at 90 frames-per-second while subjects walked on the treadmill, and convert each frame’s depth images to a single point cloud (Boppana and Anderson 2019).

The treadmill was set to an average walking pace of 1.4 m/s (Browning et al. 2006). Reflective markers were placed on the subject’s right foot and a black sock over their left foot to aid in right foot identification described later. Subjects first walked for one minute to warm-up and fall into a natural cadence. The operator then collected 10 seconds of data to capture approximately 10 steps. The data were reviewed to ensure the subject stayed in frame from heel-strike to toe-off during capture. If needed, the subject’s placement was shifted and data was collected again, up to two times.

2.3. Data Processing

For each subject, a candidate heel-strike to toe-off event was manually identified across all captures by taking into account point cloud quality due to the high computational power required to process all heel-strike to toe-off events. The depth images captured by each depth camera were processed into point clouds using the DynaMo package. From each point cloud, the right foot was isolated and transformed into a triangle mesh. Since every depth image was captured independently by the cameras, the amount and location of points which represented the foot in the data were not consistent. In addition, the captured data may have holes in the surface representing the foot. Registration of all scans to a common template represents every scan by an equal number of points, and ensures any missing points are properly interpolated. The right foot meshes were then iteratively registered using a three-step fitting process to an averaged high-quality static template scan from a previous study (Reed, Ebert, and Corner 2013). First scans were roughly aligned using a point-to-place iterative-closest-point algorithm (Chen and Medioni 1992), implemented in Open3d (Zhou, Park, and Koltun 2018). Next, the radial-basis function fitting algorithm from the GIAS2 software package (Zhang, Hislop-Jambrich, and Besier 2016) was run twice using a thin-plate spline to approximate the foot surface (Park and Reed 2015; Kim et al. 2016). The mid-stance scan from each

subject was registered first to the template, and then the registration process was run both forwards towards toe-off and backwards towards heel-strike, on a scan-by-scan basis, using the previously registered scan as a template for the next scan. Accuracy was checked by comparing registered scans against the processed scans by finding corresponding points between both, and calculating the root-mean-squared error (RMSE) between the corresponding points.

Anatomical landmarks can be reliably approximated from the registered scans (Van den Herrewegen et al. 2014). The first metatarsal head, fifth metatarsal head, and second toe landmarks were used to align all scans to be centered at the second metatarsal head, with the forward axis pointing towards the second toe. Landmarks around the metatarsal-phalangeal (MTP) joint and ankle joint were used to calculate three-dimensional ankle and MTP joint kinematics for each subject’s scans with respect to the joint angles at the subject’s mid-stance scan.

Further details on the mesh processing, registration, and joint angle calculation processes can be found in {#sec:supp}.

2.4. Model Construction

Principal component (PC) analysis is a dimensionality-reduction method commonly used to build statistical body shape models, with applications for whole-body (Reed and Parkinson 2008; Park and Reed 2015) as well as foot shape models (Conrad et al. 2019; Stanković et al. 2020). The first PC represents an axis containing the largest variance in the dataset, and each subsequent PC describes the largest variance orthogonal to the previous component’s axis. Therefore, PCs allow for a new, smaller set of orthogonal variables to be defined which represent the variance in the dataset.

Let N equal the number of total scans in the dataset, and $n = 29873$ equal the number of vertices in each registered scan. The scikit-learn module (Pedregosa et al. 2011) was used to incrementally calculate the maximum N PCs which represent the dataset. Each scan in the dataset is represented in the PC model with N PC scores. All PC scores are centered around 0, which represents the mean foot scan of the dataset containing all subjects. Each PC represents a shape mode in the SSM, where each score represents a deviation from the mean foot along the shape mode axis. The resultant PC model can be used to inverse transform a vector of length N PC scores into a 29873×3 vector, which represents the location of the vertices in the foot shape. Not all PCs need to be retained in the model since the first few principal components will explain a majority of the variance.

Subject demographic data and calculated joint angles were incorporated into the SSM by developing multivariate linear regression models based on these features. This was used to predict each PC score, which can then be inverse-transformed into a foot shape. Subject demographic data and joint angles were normalized and power-transformed to aid in regression development (Yeo and Johnson 2000). An elastic net regularization algorithm (Zou and Hastie 2005) was run for each multivariate regression to calculate normalized feature coefficients for each PC score’s regression. Two different sets of predictors were

created, one with all subject demographic data and calculated joint angles, and one with the highly-cross-correlated predictors of arch length, body-mass index, and height were removed. Six potential models were built as combinations between the number of PCs predicted which explained 95%, 97.5%, and 99.2% of the variance, and the two predictor sets.

2.5. Model Validation

All six models were validated for performance using leave-one-out cross-validation, where scans from each subject were set as the validation set, and models were trained on the remaining dataset. Model performance during validation was quantified with the root mean squared error (RMSE) of the predicted foot shape to the corresponding registered scan. A two-way RMANOVA analysis was run on the error distributions to test the effect of constructing a predictor with the different number of principal components, and between using the two variable sets. # Results {#sec:results}

A total of 1771 scans were analyzed across all 30 subjects. Each subject's stance phase including an average of 59 scans. Figure [#fig:scans] shows a set of raw and registered scans from one subject approximately 10 frames apart. All processed scans were registered to the template with a median registration accuracy of 1.044 ± 0.623 mm.

The PCA analysis of all registered scans found the first 14 PCs to represent approximately 95% of the variance, the first 29 PCs to represent approximately 97.5% of the variance, and the first 118 PCs to represent approximately 99.72% of the variance.

Figure fig. 5 shows the distribution of cross-validation RMSEs for each of the six elastic net regression models tested. RMSE distributions were visually inspected for normality. A significant difference was found between the effect of predicting different numbers of principal components ($F=1110.2$, $p<0.001$), predicting between the two variable sets ($F=5.5$, $p=0.187$), and the interaction between both factors ($F=186.9$, $p<0.001$). Significant differences were found between all three levels of the predicted number of principal components ($p\text{-adj}=0.001$) with a Tukey post-hoc HSD test. No significant difference was found between predicting with all or a selected subset of variables ($p\text{-adj}=0.829$). Therefore, the model predicting 14 principal components with the selected set of variables was selected as the best predictor as it was the simplest model with the best performance.

Figure fig. 6 shows the chosen model's normalized coefficient values for each PC. The coefficients for the sex predictor are not shown as they were calculated to be zero for every principal component.

Figure fig. 7 shows the ratio of total variance each of the first 14 principal components account for. Figure fig. 8 shows each shape mode's axis represented on the mean foot. Figure fig. 9 shows the ± 2 standard deviations of shape modes 1,2,3,4,5, and 9, overlaid on the mean foot.

3. Discussion

This study was designed to construct and evaluate a parametric statistical shape model in explaining and predicting dynamic foot morphology changes across the subject population. The model was able to predict dynamic foot shape across the subject population with a average RMSE of 5.676 ± 2.363 mm. This value is higher than the half-size step of the American shoe sizing system (Luximon and Luximon 2013), but less than inter-brand variability of shoe length and shoe width (Wannop et al. 2019). This value is lower than the RMSEs of other parametric statistical shape models that predicted static standing child body shape (mean=10.4mm) (Park and Reed 2015), dynamic shoulder deformation (mean=11.98mm) (Kim et al. 2016) and child torso shape (mean=9.5mm) (Park, Ebert, and Reed 2017). The presented model may have lower prediction errors due to the foot being a relatively smaller section of the body to model. Grant et al's model reconstructed internal foot bones with much lower RMSEs from sparse anatomical landmarks (1.21-1.66 mm for various foot segments) (Grant et al. 2020) but also used higher resolution MRI images for model training. Other efforts to create statistical foot shape models did not incorporate parametric prediction of foot shape (Conrad et al. 2019; Stanković et al. 2020).

The first, second, and fourth shape modes, accounting for a total of 81.6% of total variance, capture gross movement of the foot and ankle joint around the model's origin. Foot motion during stance is dominated by saggital plane motion of MTP plantar/dorsiflexion and ankle plantar/dorsiflexion (Leardini et al. 2007), and is captured in the first shape mode. The second and fourth shape modes capture gross changes in foot rotation from movements in the frontal and transverse planes at the MTP and ankle joints, respectively. The second shape mode also captures girth scaling at the ankle joint, affected by foot width, weight, and foot length. MTP inversion/eversion and internal/external rotation are expected to vary across the stance phase (Leardini et al. 2007), but ankle inversion/eversion and internal/external rotation seem to be highly subject-specific and not correlated to stance phase duration. This may be due to the treadmill being set to a constant speed for all subjects, which may not have been the subject's preferred walking speed. In fact, the fourth shape mode appears to be affected by foot length, which may suggest that those with longer feet might have more ankle eversion during stance phase when limited in walking speed.

The third shape mode, accounting for 6.6% of total variance, captures foot shape scaling and morphological changes at the rearfoot. Foot length scaling is captured in a negative direction along this shape mode, and thus has a negative effect from foot length. Rearfoot morphology along this shape mode has a more rounded shape in the negative direction, and a sharper shape in the positive direction. There is a positive effect for this shape mode from MTP joint flexion/extension and MTP joint pronation/supination, indicating that with MTP joint flexion and pronation, a sharper rearfoot shape is expected. This may be due to the flattening of the rearfoot when it makes contact with the ground; as

the rearfoot is lifted off the ground during MTP joint flexion, it returns to a sharper non-weight-bearing shape.

275 Midfoot girth changes are captured in the fifth shape mode, accounting for 1.6% of total variance, and are primarily affected by foot length, with slight positive effects from weight, foot width, and ankle inversion/eversion, and a slight negative effect from MTP dorsi/plantarflexion. This suggests that static midfoot girth may increase with larger foot lengths, foot widths, and weights,
280 and decrease as the foot is unloaded at heel-off. It was previously suggested that midfoot girth decreases during stance phase compared to statically standing (Grau and Barisch-Fritz 2018), most likely due to intrinsic and extrinsic foot muscle contraction (Scott and Winter 1993; Gefen et al. 2000). However, it was not noted where during stance phase midfoot girth decreases, but it can now be assumed it occurs during heel-off.
285

Subsequent principal components, accounting for 5.5% of total variance, capture more minor foot morphology variance. The seventh shape mode is affected by foot length, ankle pronation/supination, ankle dorsi/plantarflexion and ankle internal/external rotation at the calcaneus and first phalange. This shape mode may have similar mechanism to the third shape mode, where morphology is affected by loading and unloading of the foot. The ninth principal component focuses on the MTP joint region, where the positive direction increases MTP joint girth. This shape mode is affected positively by MTP joint pronation/supination and MTP joint dorsi/plantarflexion, and is affected negatively by ankle internal/external rotation, ankle pronation/supination, foot length, and foot width. This suggests that MTP joint girth may decrease with increasing foot length and foot width, but increase during heel-off. Similar mechanisms may also be occurring in the 11th, 13th, and 14th shape modes, where morphology of the metatarsals and MTP joint may be expanding during heel-off. The
290 foot is stiffened through tension in the MTP joints in order to prepare for push-off (Hicks 1954), and the MTP joints are known to move relatively within the foot during gait (Wolf et al. 2008; Lundgren et al. 2008) which may be resulting in the increased girth at the MTP joint.
295

The changes in midfoot girth and MTP joint girth may be directly mapped
300 to footwear recommendations for increased fit and comfort. The midfoot should remain supported through heel-off, as this part of the foot drives footwear plantarflexion through contact while the MTP joint is dorsiflexing. Since there was an observed decrease in midfoot girth, footwear may need to contract to ensure proper contact. Decrease in midfoot girth through heel-off may suggest further support at this area, as the midfoot is still driving shoe plantarflexion through dorsiflexion of the MTP joint. An allowance of space at the MTP joint will accommodate the increases in MTP joint girth at heel-off.
310

There are a number of limitations in this study that must be noted. The elastic-net method is able to retain cross-correlated predictors compared to the Lasso method, but still requires some bias in the dataset to be able to predict scenarios where cross-correlated predictors are independent (Zou and Hastie 2005). Therefore, the presented model may not be valid for predicting changes in morphology due to independent changes in joint angles outside of stance
315

phase, or for variance in foot width or weight compared to foot length not
320 captured in the subject population.

The model did not find any differences between male and female feet. Studies found that sex differences in foot shape after scaling for foot length are not significant (Kouchi, Kimura, and Mochimaru 2009; Barisch-Fritz et al. 2014b; Conrad et al. 2019), and that even significant differences in certain measurements are still small in magnitude (Wunderlich and Cavanagh 2001; Krauss et al. 2008). No subject demographic data was collected to account for differences in foot shape due to ethnicity (Jurca, Žabkar, and Džeroski 2019). No data was captured on the foot's plantar surface due to limitations with the scanning system; therefore no data on foot arch type and changes was captured. Data
325 captured around the toes had high noise, which necessitated the smoothing of the toes in the template to ease fitting. Future advances in 4D scanning may
330 be able to alleviate some of these concerns, and also allow for expansion of this model to foot motions with higher movement frequencies, such as running.

4. Conclusions

To the authors' knowledge, this is the first parametric statistical foot shape model that captures and reconstructs dynamic motion. The model was able to identify specific changes in foot morphology as they related to subject and kinematic parameters, and suggest increased support at the midfoot and increased volume allowance at the MTP joint. The model is able to reconstruct a full 3D model when parameter values are provided, which offers shoe and last
335 designers a design starting point, and the ability to test their designs on a range of subjects throughout stance phase. It is only expected that as 4D scanning technologies improve, the presented methodology can be used to improve the model prediction performance.

345 5. Supplemental Information

Following is more details on the mesh construction, template registration, and joint angle calculation methods.

5.1. Mesh Construction

The C++ implementation of the PointCloud Library (Rusu and Cousins 2011) was used to identify and isolate the right foot from the point set. First,
350 the point clouds were downsampled with a voxel size of 3 mm to reduce required computing power. A RANSAC algorithm (Fischler and Bolles 1981) was used to identify the flat treadmill floor with a plane model, and remove it from the point cloud. Euclidean cluster extraction was then used to detect the point clusters that make up each foot. The total color value of each point cluster was
355 used to identify the right foot from the left foot, as the left foot had a lower total color value due to the black sock. The left foot was then removed from the point cloud, leaving only the right foot for processing.

Surface reconstruction was done through Meshlab (Cignoni et al. 2008). A
360 surface mesh adds a topological layer interpreted from the pointcloud. Point
normals were calculated for the point cloud using the 10 nearest neighbors. An
APSS Marching Cubes algorithm (Guennebaud and Gross 2007; Guennebaud,
Germann, and Gross 2008) is then used with the point normals to estimate the
surface from the point cloud and construct the foot scan mesh.

365 *5.2. Foot Template Registration*

From the provided template, the toes were smoothed into a single structure
and parts of the upper shank removed to be better fit to the captured data, with
a finalized structure of 29873 points. The overall registration process follows a
370 three-step process: a rough alignment followed by two radial-basis function
(RBF) fine alignment steps

The registration process was first completed for each subject's data with a
foot scan mesh manually identified near mid-stance. A point-to-plane iterative-
closest-point (ICP) algorithm (Chen and Medioni 1992) was used to roughly
align the template foot to the scan mesh with the Open3D library (Zhou, Park,
375 and Koltun 2018).

Corresponding points between both the scan mesh and the ICP-aligned tem-
plate were found using a radial-search KD-Tree implemented in the Open3D li-
brary (Zhou, Park, and Koltun 2018). Any points on the scan mesh which were
380 not within 1 cm of a corresponding point on the aligned template were deleted;
these points represented parts of the treadmill floor which were missed in the
RANSAC identification and parts of the upper shank. Similarly, any points on
the template not within 1cm of a corresponding point on the scan mesh were
temporarily set aside from the template; these points correspond to those near
holes in the scan mesh which would be refilled in later processing

385 Thin-plate spline RBFs have been used to surface fit templates to scanned
body shapes (Park and Reed 2015; Kim et al. 2016), and so were used in two
stages in this research. A first-pass RBF registration, using a thin-plate spline
for interpolation, was done between the template and the scan using the GIAS2
package (Zhang, Hislop-Jambrich, and Besier 2016) To prevent overfitting of the
390 RBF to the noise on the edges of the captured pointcloud, a maximum of five
iterations were done on the first-pass RBF registration process. The first-pass
registered RBF template was then appended with the points previously removed
from the template. This intermediate template represents the template fitted to
the known scan data, with any unknown sections (e.g. holes in the scan data),
395 taking the value of the template. However, the disparity between the known
and unknown sections created major discrepancies in the morphed template not
representative of the scan data.

A second-pass RBF registration was done from the ICP-aligned template
to the intermediate template with the same parameters as the first-pass regis-
400 tration. This smooths out the unknown sections representing holes in the scan
data with the surrounding known sections. The second-pass registered template
was saved as the final registered template.

Following the registration of the mid-stance scan, the process was repeated both forwards towards toe-off and backwards toward heel-strike on a scan-by-scan basis. In this iterative fashion, the previous scan's registered template was used as the template for the following scan. During the iterative registration process, the RBF alignment was only conducted for one iteration for both the first-pass and second-pass to prevent over-fitting.

5.3. Joint Angle Calculation

The original template identified the lateral malleolus, medial malleolus, 1st metatarsal head, 5th metatarsal head, and 2nd toe landmarks as certain vertices. New landmark vertices for the lateral shank and medial shank were manually picked on the template.

Post-registration scans were aligned to a common coordinate frame based around the toes. The origin was defined as the point along the vector from the 1st metatarsal head landmark to the 5th metatarsal head landmark which is orthogonal to the second phalange. From the origin, the x-axis, was defined as pointing towards the 2nd toe. The y-axis, was pointing towards the 1st metatarsal. The z-axis was the cross-product of both x- and y-axes. This coordinate system also served as the static coordinate system for the MTP joint.

The ankle joint center was defined as the midpoint between the medial and lateral malleous. The ankle's local z-axis is aligned with the shank center, defined as the center between the lateral shank and medial shank landmarks. The ankle's local y-axis is aligned from the shank center to the lateral malleolus. The ankle's x-axis is the cross-product of the y- and z- axis.

Static reference angles were taken from these coordinate systems at mid-stance. For the ankle joint, the z-axis served as the internal/external rotation axis, the y-axis as the dorsi/plantarflexion axis, and the x-axis as the inversion/eversion axis. Since the model's origin was at the toes, the calculation for MTP dorsi/plantarflexion was modified. The new local MTP joint coordinate system had the x-axis defined as pointing from the ankle joint center to the MTP joint center, as such the y-axis represented MTP dorsi/plantarflexion. Since there is little flexibility in the transverse and frontal planes of the MTP joint, the x-axis therefore represented whole foot inversion/eversion, and the z-axis represented whole foot internal/external rotation around the origin. MTP and ankle joint angles were calculated for every other scan as the Euler angle difference from the static joint coordinate system around each axis. The global and local coordinate systems are summarized in fig. 3

Figures

Allen, Brett, Brian Curless, and Zoran Popović. 2003. "The space of human body shapes: Reconstruction and parameterization from range scans." *ACM Transactions on Graphics* 22 (3): 587–94. <https://doi.org/10.1145/882262.882311>.



Figure 1: Capture setup of 6 Intel RealSense D415 Depth Cameras placed around a treadmill. The checkerboard shown was used to calibrate the cameras using the DynaMo package

- 445 Anguelov, Dragomir, Praveen Srinivasan, Daphne Koller, Sebastian Thrun,
Jim Rodgers, and James Davis. 2005. “SCAPE: Shape Completion and An-
imation of People.” *ACM Transactions on Graphics* 24 (3): 408–16. <https://doi.org/10.1145/1073204.1073207>.
- 450 Barisch-Fritz, Bettina, Timo Schmelzpfenning, Clemens Plank, Tobias Hein,
and Stefan Grau. 2014a. “The effects of gender, age, and body mass on dy-
namic foot shape and foot deformation in children and adolescents.” *Footwear
Science* 6 (1): 27–39. <https://doi.org/10.1080/19424280.2013.834982>.
- 455 ———. 2014b. “The effects of gender, age, and body mass on dynamic foot
shape and foot deformation in children and adolescents.” *Footwear Science* 6
(1): 27–39. <https://doi.org/10.1080/19424280.2013.834982>.
- Boppana, Abhishektha, and Allison P Anderson. 2019. “DynaMo: Dynamic
Body Shape and Motion Capture with Intel RealSense Cameras.” *The Journal
of Open Source Software* 4 (41). <https://doi.org/10.21105/joss.01466>.
- Browning, Raymond C., Emily A. Baker, Jessica A. Herron, and Rodger
Kram. 2006. “Effects of obesity and sex on the energetic cost and preferred
speed of walking.” *Journal of Applied Physiology* 100 (2): 390–98. <https://doi.org/10.1152/japplphysiol.00767.2005>.
- 460 Chen, Yan, and Gerard Medioni. 1992. “Object modelling by registration of
multiple range images.” *Image and Vision Computing* 10 (3): 2724–9. <https://graphics.stanford.edu/%7B~%7Dsmr/ICP/comparison/chen-medioni-align-rob91.pdf>.

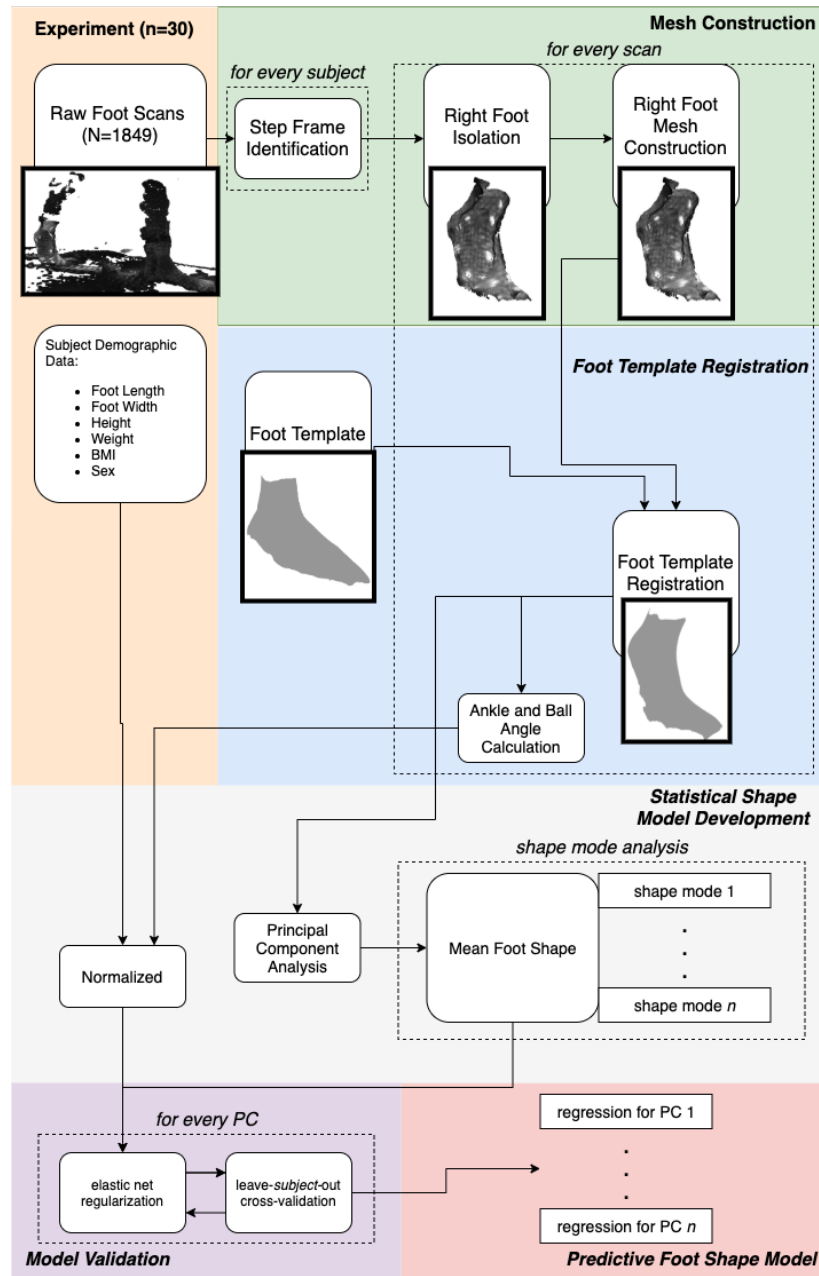


Figure 2: Flowchart of processing steps for statistical shape model creation

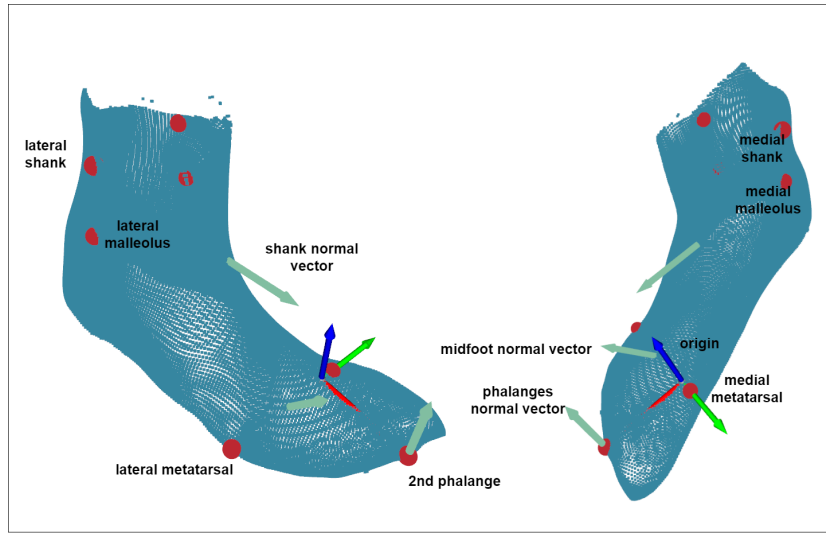


Figure 3: Anatomical landmarks, coordinate system, and vectors defining anatomical segments of a registered scan

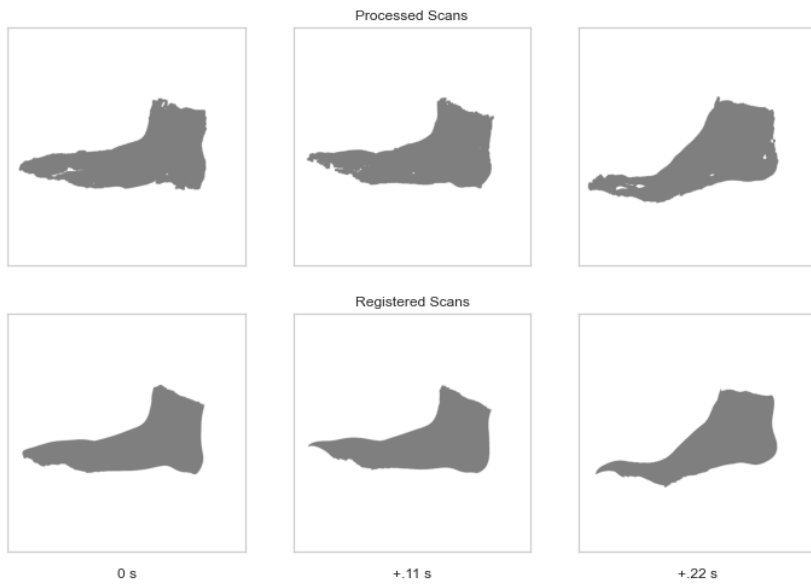


Figure 4: Processed and registered scans of one subject during heel-off, shown 10 frames (.11 seconds) apart

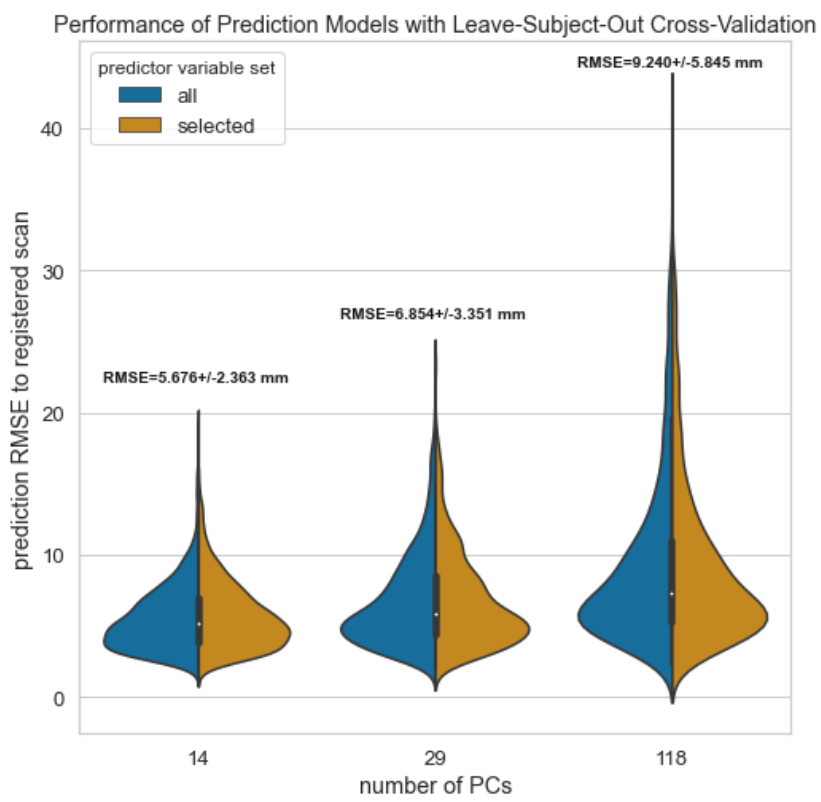


Figure 5: Distribution of errors across the various prediction models leave-subject-out cross-validation results. Model RMSE mean and standard deviation are shown above each distribution

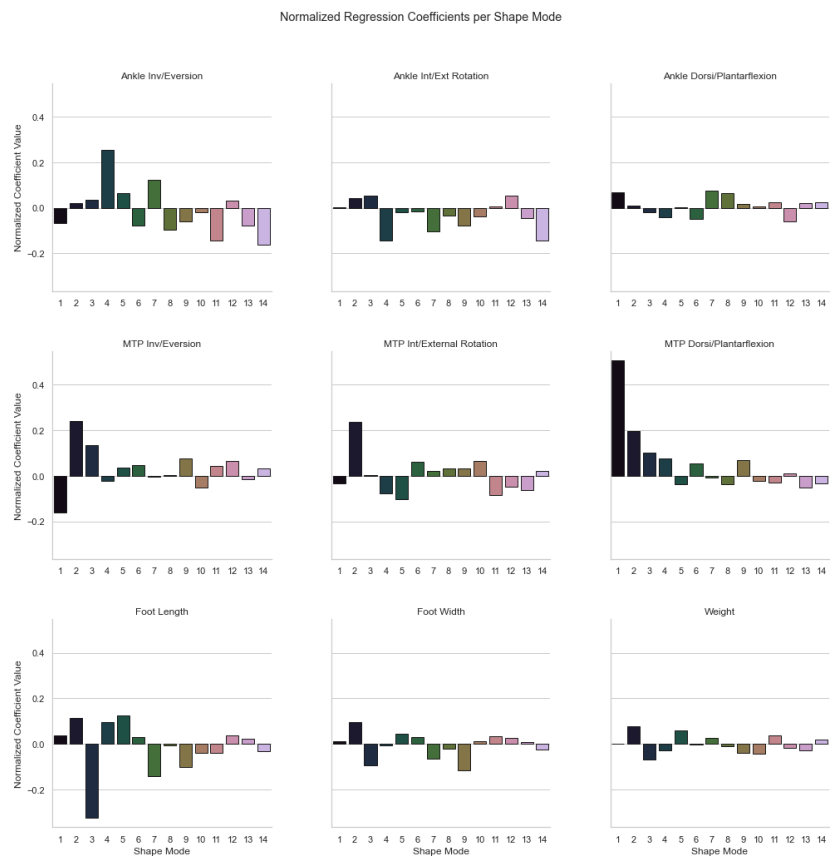


Figure 6: Normalized coefficient values for each principal component.

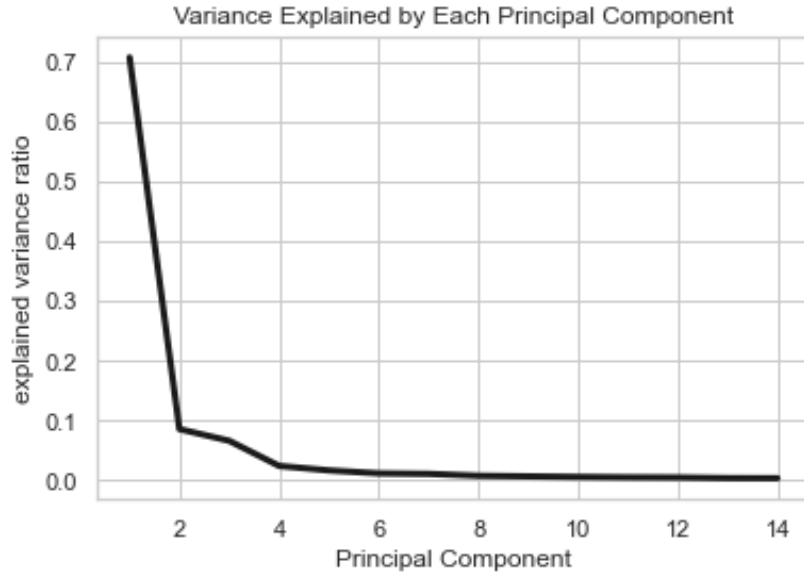


Figure 7: Ratio of variance explained by each of the first 14 principal components.

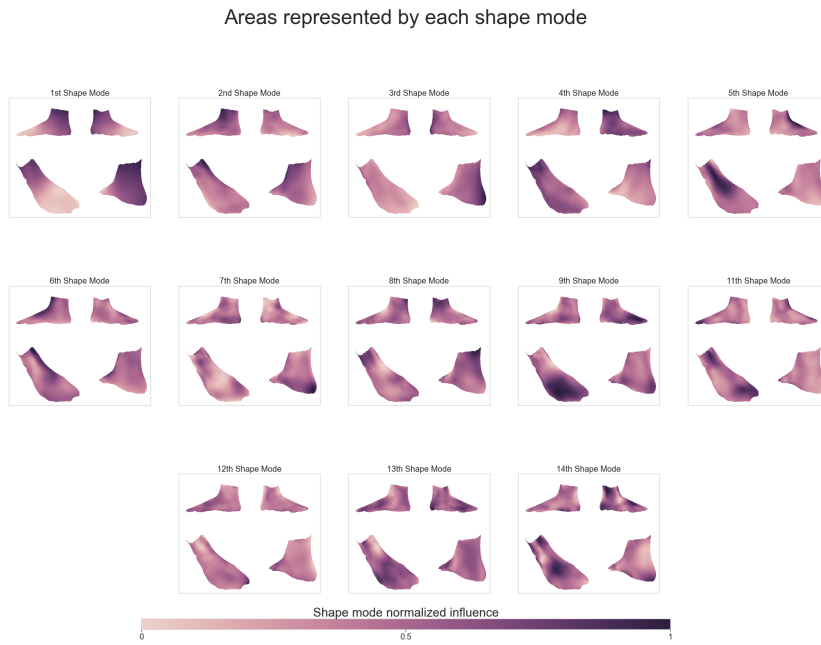


Figure 8: Each shape mode's axis represented as a heatmap overlaid on the mean foot and shown from 4 different point-of-views. The darker regions are where the shape mode accounts for more variance at those vertices.

Shape Mode Variation

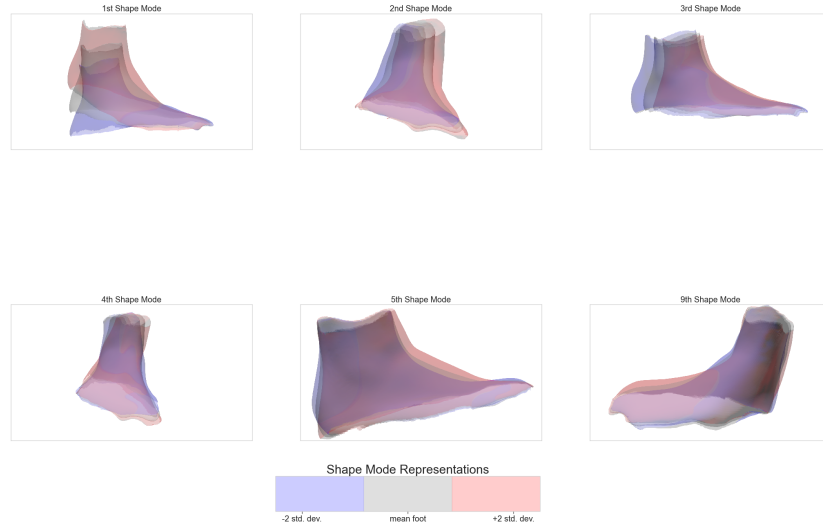


Figure 9: Variation along each shape mode's axis, overlaid on the mean foot. The point-of-view is set to highlight the major variance along each shape mode's axis.

Cignoni, P., M. Callieri, M. Corsini, M. Dellepiane, F. Ganovelli, and G. Ranzuglia. 2008. “MeshLab: An open-source mesh processing tool.” *6th Eurographics Italian Chapter Conference 2008 - Proceedings*, 129–36.

Conrad, Bryan P., Michael Amos, Irene Sintini, Brian Robert Polasek, and Peter Laz. 2019. “Statistical shape modelling describes anatomic variation in the foot.” *Footwear Science* 11 (sup1): S203–S205. <https://doi.org/10.1080/19424280.2019.1606334>.

Dobson, Jessica A., Diane L. Riddiford-Harland, Alison F. Bell, and Julie R. Steele. 2018. “The three-dimensional shapes of underground coal miners’ feet do not match the internal dimensions of their work boots.” *Ergonomics* 61 (4): 588–602. <https://doi.org/10.1080/00140139.2017.1397201>.

Fischler, Martin A., and Robert C. Bolles. 1981. “Random sample consensus: A Paradigm for Model Fitting with Applications to Image Analysis and Automated Cartography.” *Communications of the ACM* 24 (6): 381–95. <https://doi.org/10.1145/358669.358692>.

Gefen, A., M. Megido-Ravid, Y. Itzhak, and M. Arcan. 2000. “Biomechanical analysis of the three-dimensional foot structure during gait: A basic tool for clinical applications.” *Journal of Biomechanical Engineering* 122 (6): 630–39. <https://doi.org/10.1115/1.1318904>.

Giles, Eugene, and Paul H. Vallandigham. 1991. “Height Estimation from Foot and Shoeprint Length.” *Journal of Forensic Sciences* 36 (4): 13129J.

- <https://doi.org/10.1520/jfs13129j>.
- 490 Gordon, Claire C., Cynthia L. Blackwell, Bruce Bradtmiller, Joseph L. Parham, Patricia Barrientos, Stephen P. Paquette, Brian D. Corner, et al. 2014. “2012 Anthropometric Survey of U.S. Army Personnel: Methods and Summary Statistics.” Natick, MA: ARMY NATICK SOLDIER RESEARCH DEVELOPMENT AND ENGINEERING CENTER MA. <https://apps.dtic.mil/docs/citations/ADA611869>.
- 495 Grant, Tamara M., Laura E. Diamond, Claudio Pizzolato, Bryce A. Killen, Daniel Devaprakash, Luke Kelly, Jayishni N. Maharaj, and David J. Saxby. 2020. “Development and validation of statistical shape models of the primary functional bone segments of the foot.” *PeerJ* 2020 (2): e8397. <https://doi.org/10.7717/peerj.8397>.
- 500 Grau, Stefan, and Bettina Barisch-Fritz. 2018. “Improvement of safety shoe fit - evaluation of dynamic foot structure.” *Footwear Science* 10 (3): 179–87. <https://doi.org/10.1080/19424280.2018.1529062>.
- 505 Guennebaud, Gaël, Marcel Germann, and Markus Gross. 2008. “Dynamic sampling and rendering of algebraic point set surfaces.” *Computer Graphics Forum* 27 (2): 653–62. <https://doi.org/10.1111/j.1467-8659.2008.01163.x>.
- Guennebaud, Gaël, and Markus Gross. 2007. “Algebraic point set surfaces.” *Proceedings of the ACM SIGGRAPH Conference on Computer Graphics*. <https://doi.org/10.1145/1275808.1276406>.
- Hicks, J. H. 1954. “The mechanics of the foot II. The plantar aponeurosis and the arch.” *Journal of Anatomy* 88 (1): 25–30.
- 510 Jurca, Ales, and Saso Dzeroski. 2013. “Length dispersion of shoes labelled with the same size in the UK shoe-size system.” *Footwear Science* 5 (SUPPL. 1): 2–5. <https://doi.org/10.1080/19424280.2013.799543>.
- Jurca, Ales, Jure Žabkar, and Sašo Džeroski. 2019. “Analysis of 1.2 million foot scans from North America, Europe and Asia.” *Scientific Reports* 9 (1): 1–10. <https://doi.org/10.1038/s41598-019-55432-z>.
- 515 Kessler, Sarah E., Glen A. Lichtwark, Lauren K. M. Welte, Michael J. Rainbow, and Luke A. Kelly. 2020. “Regulation of foot and ankle quasi-stiffness during human hopping across a range of frequencies.” *Journal of Biomechanics*, 109853. <https://doi.org/10.1016/j.jbiomech.2020.109853>.
- 520 Kim, K. Han, Karen S. Young, Yaritza Bernal, Abhishektha Boppana, Linh Q. Vu, Elizabeth A. Benson, Sarah Jarvis, and Sudhakar L. Rajulu. 2016. “A Parametric Model of Shoulder Articulation for Virtual Assessment of Space Suit Fit.” In *Proceedings of the 7th International Conference on 3D Body Scanning Technologies*, 201–7. Lugano, Switzerland. <https://doi.org/10.15221/16.201>.
- Kouchi, Makiko, Makoto Kimura, and Masaaki Mochimaru. 2009. “Deformation of foot cross-section shapes during walking.” *Gait and Posture* 30 (4): 482–86. <https://doi.org/10.1016/j.gaitpost.2009.07.113>.
- 530 Krauss, I., S. Grau, M. Mauch, C. Maiwald, and T. Horstmann. 2008. “Sex-related differences in foot shape.” *Ergonomics* 51 (11): 1693–1709. <https://doi.org/10.1080/00140130802376026>.

- Krauss, Inga, Gordon Valiant, Thomas Horstmann, and Stefan Grau. 2010.
535 "Comparison of female foot morphology and last design in athletic footwear-
are men's lasts appropriate for women?" *Research in Sports Medicine* 18 (2):
140–56. <https://doi.org/10.1080/15438621003627216>.
- Leardini, A., M. G. Benedetti, L. Berti, D. Bettinelli, R. Nativo, and S. Giannini. 2007. "Rear-foot, mid-foot and fore-foot motion during the stance phase of gait." *Gait and Posture* 25 (3): 453–62. <https://doi.org/10.1016/j.gaitpost.2006.05.017>.
- Lundgren, P., C. Nester, A. Liu, A. Arndt, R. Jones, A. Stacoff, P. Wolf, and A. Lundberg. 2008. "Invasive in vivo measurement of rear-, mid- and forefoot motion during walking." *Gait and Posture* 28 (1): 93–100. <https://doi.org/10.1016/j.gaitpost.2007.10.009>.
- Luo, Geng, Pro Stergiou, Jay Worobets, Benno Nigg, and Darren Stefanyshyn. 2009. "Improved footwear comfort reduces oxygen consumption during running." *Footwear Science* 1 (1): 25–29. <https://doi.org/10.1080/19424280902993001>.
- Luximon, Y., and A. Luximon. 2013. "Sizing and grading of shoe lasts." *Handbook of Footwear Design and Manufacture*, 197–215. <https://doi.org/10.1533/9780857098795.3.197>.
- Martínez-Martínez, José M., José D. Martín-Guerrero, Emilio Soria-Olivas, José A. Bernabeu, Pablo Escandell-Montero, Rafael Hernández Stark, Antonio J. Serrano-López, and Enrique Montiel. 2017. "Use of SOMs for footwear comfort evaluation." *Neural Computing and Applications* 28 (7): 1763–73. <https://doi.org/10.1007/s00521-015-2139-x>.
- Mündermann, A., D. J. Stefanyshyn, and B. M. Nigg. 2001. "Relationship between footwear comfort of shoe inserts and anthropometric and sensory factors." *Medicine and Science in Sports and Exercise* 33 (11): 1939–45. <https://doi.org/10.1097/00005768-200111000-00021>.
- Oladipo, G, I Bob-Manuel, and G Ezenatein. 2008. "Different Weight Bearing Conditions Amongst Nigerians." *The Internet Journal of Biological Anthropology* 3 (1): 1–7.
- Park, Byoung Keon D., Sheila Ebert, and Matthew P. Reed. 2017. "A parametric model of child body shape in seated postures." *Traffic Injury Prevention* 18 (5): 533–36. <https://doi.org/10.1080/15389588.2016.1269173>.
- Park, Byoung Keon, and Matthew P. Reed. 2015. "Parametric body shape model of standing children aged 3–11 years." *Ergonomics* 58 (10): 1714–25. <https://doi.org/10.1080/00140139.2015.1033480>.
- Pedregosa, Fabian, Ron Weiss, Matthieu Brucher, Gaël Varoquaux, Alexandre Gramfort, Vincent Michel, Bertrand Thirion, et al. 2011. "Scikit-learn: Machine Learning in Python." *Journal of Machine Learning Research* 12 (85): 2825–30. <https://doi.org/10.1145/2786984.2786995>.
- Price, Carina, and Christopher Nester. 2016. "Foot dimensions and morphology in healthy weight, overweight and obese males." *Clinical Biomechanics* 37: 125–30. <https://doi.org/10.1016/j.clinbiomech.2016.07.003>.
- Reed, Matthew P, Sheila M Ebert, and Brian D Corner. 2013. "Statistical Analysis to Develop a Three-Dimensional Surface Model of a Midsize-Male

- Foot.” October.
- 580 Reed, Matthew P., and Matthew B. Parkinson. 2008. “Modeling variability in torso shape for chair and seat design.” *Proceedings of the ASME Design Engineering Technical Conference* 1 (PARTS A AND B): 561–69. <https://doi.org/10.1115/DETC2008-49483>.
- 585 Reed, M. P., Ulrich Raschke, Rishi Tirumali, and M. B. Parkinson. 2014. “Developing and Implementing Parametric Human Body Shape Models in Ergonomics Software.” *3rd Digital Human Modeling Symposium*, no. 1: 1–8.
- 590 Riebe, Deborah, Barry A. Franklin, Paul D. Thompson, Carol Ewing Garber, Geoffrey P. Whitfield, Meir Magal, and Linda S. Pescatello. 2015. “Updating ACSM’s recommendations for exercise preparticipation health screening.” *Medicine and Science in Sports and Exercise* 47 (11): 2473–9. <https://doi.org/10.1249/MSS.0000000000000664>.
- 595 Rusu, Radu Bogdan, and Steve Cousins. 2011. “3D is here: Point Cloud Library (PCL).” In *Proceedings - Ieee International Conference on Robotics and Automation*. Shanghai, China. <https://doi.org/10.1109/ICRA.2011.5980567>.
- 600 Scott, Stephen H., and David A. Winter. 1993. “Biomechanical model of the human foot: Kinematics and kinetics during the stance phase of walking.” *Journal of Biomechanics* 26 (9): 1091–1104. [https://doi.org/10.1016/S0021-9290\(05\)80008-9](https://doi.org/10.1016/S0021-9290(05)80008-9).
- 605 “Standard Practice for Fitting Athletic Footwear.” 2017. ASTM. <https://doi.org/10.1520/F0539-01R11.2>.
- 610 Stanković, Kristina, Toon Huysmans, Femke Danckaers, Jan Sijbers, and Brian G. Booth. 2020. “Subject-specific identification of three dimensional foot shape deviations using statistical shape analysis.” *Expert Systems with Applications* 151 (August): 113372. <https://doi.org/10.1016/j.eswa.2020.113372>.
- 615 Tomassoni, Daniele, Enea Traini, and Francesco Amenta. 2014. “Gender and age related differences in foot morphology.” *Maturitas* 79 (4): 421–27. <https://doi.org/10.1016/j.maturitas.2014.07.019>.
- 620 Van den Herrewegen, Inge, Kris Cuppens, Mario Broeckx, Bettina Barisch-Fritz, Jos Vander Sloten, Alberto Leardini, and Louis Peeraer. 2014. “Dynamic 3D scanning as a markerless method to calculate multi-segment foot kinematics during stance phase: Methodology and first application.” *Journal of Biomechanics* 47 (11): 2531–9. <https://doi.org/10.1016/j.jbiomech.2014.06.010>.
- 625 Wannop, John W., Darren J. Stefanyshyn, Robert B. Anderson, Michael J. Coughlin, and Richard Kent. 2019. “Development of a Footwear Sizing System in the National Football League.” *Sports Health* 11 (1): 40–46. <https://doi.org/10.1177/1941738118789402>.
- 630 Wolf, P., A. Stacoff, A. Liu, C. Nester, A. Arndt, A. Lundberg, and E. Stuessi. 2008. “Functional units of the human foot.” *Gait and Posture* 28 (3): 434–41. <https://doi.org/10.1016/j.gaitpost.2008.02.004>.
- 635 Wunderlich, R. E., and P. R. Cavanagh. 2001. “Gender differences in adult foot shape: Implications for shoe design.” *Medicine and Science in Sports and*

- 625 *Exercise* 33 (4): 605–11. <https://doi.org/10.1097/00005768-200104000-00015>.
- 630 Xiong, Shuping, Ravindra S. Goonetilleke, Jianhui Zhao, Wenyan Li, and Channa P. Witana. 2009. “Foot deformations under different load-bearing conditions and their relationships to stature and body weight.” *Anthropological Science* 117 (2): 77–88. <https://doi.org/10.1537/ase.070915>.
- 635 Yeo, In-Kwon, and Richard A Johnson. 2000. “A new family of power transformations to improve normality or symmetry.” *Biometrika* 87 (4): 954–59. <https://doi.org/10.1093/biomet/87.4.954>.
- 640 Zelik, Karl E., and Eric C. Honert. 2018. “Ankle and foot power in gait analysis: Implications for science, technology and clinical assessment.” *Journal of Biomechanics* 75: 1–12. <https://doi.org/10.1016/j.jbiomech.2018.04.017>.
- 645 Zhang, Ju, Jacqui Hislop-Jambrich, and Thor F. Besier. 2016. “Predictive statistical models of baseline variations in 3-D femoral cortex morphology.” *Medical Engineering and Physics* 38 (5): 450–57. <https://doi.org/10.1016/j.medengphy.2016.02.003>.
- 650 Zhou, Qian-Yi, Jaesik Park, and Vladlen Koltun. 2018. “Open3D: A Modern Library for 3D Data Processing.” *arXiv:1801.09847*. <http://arxiv.org/abs/1801.09847>.
- 655 Zou, Hui, and Trevor Hastie. 2005. “Regularization and variable selection via the elastic net.” *Journal of the Royal Statistical Society. Series B: Statistical Methodology* 67 (2): 301–20. <https://doi.org/10.1111/j.1467-9868.2005.00503.x>.

Acknowledgements

650 The authors would like to thank Rodger Kram for allowing the use of his lab space and treadmill, and Wouter Hoogkamer for helping get setup in the lab. The authors would also like to thank Steven Priddy for suggesting the methodology for isolating the right foot from the 4D scans. The authors are also gracious to Brian Corner and Matthew Reed for providing a high-quality averaged foot-scan to be used as the template. for registration.

655 **References**